Water Vapor Binding on Organic Matter-Coated Minerals

W. Cheng, K. Hanna, J. -F. Boily

Water vapor binding on
organic matter-coated minerals

W. Cheng[1,2], K. Hanna[1], J.-F. Boily[2]

[1]Univ Rennes, École Nationale Supérieure de Chimie de Rennes, CNRS, ISCR – UMR6226, F-35000

Rennes, France

2. Department of Chemistry, Umeå University, SE-901 87 Umeå, Sweden

ABSTRACT

Atmospheric water vapor binding to soils is a key process driving water availability in unsaturated terrestrial environments. Using a representative hydrophilic iron oxyhydroxide, this study highlights key mechanisms through which water vapor (*i*) adsorbs and (*ii*) condenses at mineral surfaces coated with Leonardite humic acid (LHA). Microgravimetry and vibrational spectroscopy showed that liquid-like water forms in the three-dimensional array of mineral-bound LHA when present at total C/Fe ratios well exceeding ~240 mg C per g Fe. Below these loadings, minerals become even less hydrophilic than in the absence of LHA. This lowering in hydrophilicity is caused by the complexation of LHA water-binding sites to mineral surfaces, and possibly by conformational changes in LHA structure removing available condensation environments for water. An empirical relationship predicting the dependence of water adsorption densities on LHA loadings was developed from these results. Together with the molecular-level description provided in this work, this relationship should guide efforts in predicting water availability, and thereby occurrences of water-driven geochemical processes in terrestrial environments.

1. INTRODUCTION

Soil hydrophobicity is a key parameter that describes the extent to which water-based geochemical reactions can proceed, and can be used in environmental monitoring and soil quality assessment.[1] This concept is a manifestation of the ability to which water vapor flowing through unsaturated soils (*e.g.* vadose zones) can form thin water films and droplets at and between mineral grains. Knowledge of the propensity of formation of these aqueous environments is consequently essential for predicting water availability, as well as geochemical aqueous reactions taking place within the microscopic solvation environments of water films and droplets.

Understanding the fate of water binding to soils also requires knowledge of the intervening roles of natural organic matter (NOM). Of common occurrence in soils,[2–4] NOM strongly reacts with mineral surfaces via chemical and/or physical adsorption reactions involving their hydrophilic functional groups (*e.g.* carboxylates, phenolates, amines), as well as by van der Waals hydrophobic interactions, and cation bridging.[5–9] These organic coatings have a strong propensity to alter the hydrophilicity of mineral surfaces, the extent to which could be determined by the type and concentration of functional groups exposed at the mineral-organic/water vapor interface. Mineral-bound NOM can also alter surface properties of minerals,[5] and have direct consequences on the mobility and fate of other contaminants, such as organic contaminants and heavy metals,[10–14] through an interconnected network of water films/droplets localized on organic-coated mineral grains.

Although the concept of soil mineral hydrophobicity is well recognized and its influence on organic compound transport studied,[1,11,15] its underlying mechanisms remain misunderstood. Still, strong correlations between soil hydrophobicity and soil organic matter[16] or mineral-sorbed humic substances have been identified.[15] Building upon our recent work on water vapor binding on minerals[17–22] and the thermochemical stability of NOM mineral coatings,[20] this work uses microgravimetry and vibrational spectroscopy to explain and predict water vapor binding to mineral-NOM mixtures. This was achieved by focusing on a model system consisting of Leonardite humic acid (LHA), a representative hydrophilic NOM, and goethite (α-FeOOH), a nanosized mineral with key roles in NOM and contaminant mobility in terrestrial and aquatic environments.[23–26]

85

2. MATERIALS AND METHODS

2.1. Materials

Goethite was synthesized by hydrothermal conversion of a freshly precipitated ferric oxyhydroxide at 60 °C for 72 h.[27,28] The starting material was made by drop-wise (1 mL/min) addition of 500 mL of a 0.5 M ferric nitrate solution ($Fe(NO_3)_3 \cdot 9H_2O$) to a continuously stirred 400 mL of 2.5 M sodium hydroxide solution in a $N_2(g)$ atmosphere. The resulting goethite was dialyzed (Spectra/Por membrane 2) against ultrapure water. The water was changed every day until its conductivity was lower than 1 µS/cm. The suspensions were stored in polypropylene containers at 4 °C for further use. Goethite purity was confirmed by X-ray diffraction (XRD) with a PANalytical X'Pert Pro X-ray diffractometer with Cu Ka radiation (c = 1.5406 Å) at 2θ range=10–65º (Figure S1).The B.E.T. specific surface area of the synthetic goethite (89.6 m^2/g) was determined on a Micromeritics AutoPore IV 9500 surface area analyzer, and was calculated from 90-point adsorption/desorption $N_2(g)$ isotherms before degassing overnight at 105°C under a stream of dry $N_2(g)$.

Leonardite Humic Acid Standard (1S104H) was purchased from the International Humic Substance Society. A LHA stock solution (2 g/ L, 1276 mg C/L) was prepared by dissolving 2 g LHA in 100 mL of 1 M NaOH, then diluted to 1 L with ultrapure water.

2.2 NOM batch adsorption experiments

All NOM adsorption experiments were conducted in the absence of background electrolyte ions, and under an atmosphere of humidified $N_2(g)$. This minimized any competitive adsorption reactions that would occur under dry conditions.

A 320 µL aliquot of a goethite (24.80 g/L, specific surface area: 89.6 m^2/g) aqueous suspension was mixed with 19.6 mL diluted LHA solutions (1.276 to 1276 mg C/L) in 50 mL polyethylene centrifuge tubes to achieve C/Fe (w/w) ratios in the 0.005−5 range. The suspensions were then adjusted to pH 5.0 with a pH meter by addition of small volumes of 1.0 M HCl or NaOH and equilibrated on an end-to-end rotator at 25 ± 1 °C for 48 h. Next, the suspension was centrifuged at ~2000 g for 15 min, the supernatants were filtered (0.2 μm) and

113   the final soluble C concentrations were analyzed using a TOC analyzer (Shimadzu TOC-VCSH). The

114   centrifuged wet pastes were analyzed by FTIR as described in Section 2.3.

115

2.3 Dynamic Vapor Sorption

117   The Dynamic Vapor Sorption (DVS) technique was used to trigger water vapor binding on initially dry

118   LHA-goethite assemblages. Water binding was monitored in two sets of independent experiments using (1)

119   Fourier Transform InfraRed (FTIR) spectroscopy, and (2) gravimetry by Quartz Crystal Microbalance (QCM).

120

121   For both experiments, water vapor was generated by mixing humid $N_2(g)$ and dry $N_2(g)$ in different

122   proportions using mass flow controllers (MKS, 179A). The total flow rate was always 200 standard cubic

123   centimeters per minute (sccm), and water vapor pressures were continuously measured using a Non

124   Dispersible InfraRed device (LI-7000, Licor Inc). Preliminary FTIR and QCM experiments demonstrated that

125   a 30 min equilibration period under a constant water vapor pressure was well sufficient to achieve equilibrium

126   with respect to water vapor binding on the LHA-goethite assemblages.

127

2.3.1 FTIR

129   Centrifuged wet pastes were transferred onto a diamond window of an Attenuated Total Reflectance (ATR)

130   cell (Golden Gate, single-bounce) and dried in the analytical chamber of a FTIR spectrometer under a flow of

131   200 sccm dry $N_2(g)$. FTIR spectra were collected during the drying period until all O−H stretching and bending

132   modes of free water disappeared. DVS experiments were then carried out on the resulting dry mineral film in

133   a closed-loop flow-through reaction cell, and exposed to water vapor pressures from 0 to 19 Torr (80% R.H.)

134   at 25 ± 1 °C.

135

136   FTIR spectra were continuously collected in situ with a Bruker Vertex 70/V FTIR spectrometer, equipped

137   with a DLaTGS detector. All spectra were collected in the $600 − 4000$ cm^{-1} range at a resolution of 4.0 cm^{-1}

138   and at a forward/reverse scanning rate of 10 Hz. Each spectrum was an average of 250 scans. The Blackman-

139   Harris 3-term apodization function was used to correct phase resolution.

140

141   *2.3.2 QCM*

142   A gold-coated quartz resonator operating at 10 MHz was used for QCM measurements (eQCM 10M,

143   Gamry Instruments Inc.). The time-independent serial resonance frequency (f_s) of the quartz resonator exposed

144   to a flow of 200 sccm dry $N_2(g)$ was first measured to obtain the correct baseline of the empty cell. A dilute

145   aqueous suspension of the LHA-goethite assemblage was pipetted on the gold area of the resonator, then dried

146   under the same flow of $N_2(g)$. The resulting f_s was used to obtain the mass of the dry sample. A DVS

147   experiment was then initiated to expose the sample to water vapor pressures from 0 to 19 Torr.

148

149   Changes in frequency (Δf) of the quartz resonator were converted to changes in sample mass (Δm) using

150   the Sauerbrey equation:[29]

151
$$\Delta f = -\frac{2f_0^2}{A\sqrt{\rho_q \mu_q}}\Delta m \quad (1)$$

152   In this equation f_0 is the resonant frequency of empty cell, A is the piezoelectrically active crystal area of the

153   gold-coated quartz crystal (0.205 cm^2), ρ_q is the density quartz (2.648 g/cm^3) and μ_q is shear modulus of quartz

154   (2.947 $\times$ 10^{11} g/cm·s^2).

155

156   *2.3.3 Water Vapor Adsorption and Condensation Modeling*

157   Water vapor uptake by goethite and LHA sites was modeled using an adaptation of the model of Do &

158   Do[30], which we had previously[31] shown to account for (*i*) *adsorption* and (*ii*) and *condensation* phenomena in

159   mineral powders:

160

161
$$C_\mu = S_o\frac{K_f\sum_1^{n=\beta+1}np_w{}^n}{1+K_f\sum_1^{n=\beta+1}p_w{}^n} + C_{\mu s}\frac{K_\mu\sum_1^{n=\alpha+1}p_w{}^n}{K_\mu\sum_1^{n=\alpha+1}p_w{}^n+\sum_1^{n=\alpha+1}p_w{}^{n-1}} \qquad (2)$$

162

163   This equation predicts the total water condensation (C_μ) as a function of the reduced partial pressure of water

164   ($p_w=p/p_{sat}$; where p_{sat} is the saturation pressure) in terms of the aforementioned *adsorption* (left-hand term)

165   and *condensation* (right-hand term) regimes. Parameters for each regime include water-binding site densities

166   for *adsorption* (S_o) and *condensation* ($C_{\mu s}$) with their respective association constants (K_f, K_μ) and hydration

167   numbers (β, α).

168   The *adsorption* term accounts for hydrogen binding of water molecules onto mineral and LHA surface

169   sites. It is B.E.T.-type equation[32] which is however forced to plateau at $p_w \rightarrow 0$ by setting $\beta=2$. This value

170   denotes that a (hydr)oxo group can be involved in 2 (donating and/or accepting) hydrogen bonds, which is

171   average hydration number that we retrieved in previous molecular modeling of water adsorption on various

172   metal (oxy)hydroxides.[31] The c*ondensation* pertains, in turn, to the condensation of water in the nano-/micro-

173   porous environments of the mineral-LHA mixture. It is triggered only when a nominal population of water

174   (nano)clusters (*e.g.* $\alpha = 8$) is exceeded[30]. While the data on hand could not be used to unambiguously constrain

175   *condensation* parameters of Eq. 2, the shape of the modelled curve nonetheless provide the possibility to

176   extract the *adsorption* term, which is central for understanding the intrinsic affinity of water to LHA-bound

177   goethite. Finally, we also used this equation to decompose the adsorption isotherm of LHA on goethite.

178

179

180

181

182

183

3. *RESULTS AND DISCUSSIONS*

184

185   LHA binding at goethite surfaces follows a Type II[33] adsorption isotherm loading (Figure 1), that can be

186   characterized as an adsorption regime at low LHA concentrations, and a precipitation-like regime at high LHA.

187   Maximal adsorption values under the adsorption regime are the equivalent of ~56 C atoms/nm^2, or ~3.7 times

188   the total crystallographic oxygen site density (~15 sites/nm^2)[27,34,35]. From these results, we estimate that the

189   goethite surface should be already covered in LHA at total C/Fe > 0.05. The highest LHA loadings (C/Fe=5;

190   220 adsorbed C atoms/nm^2) suggest a precipitation-like regime possibly triggered by LHA-LHA interactions,

191   and therefore in the establishment of LHA bulk environments entirely covering the goethite surface.


192
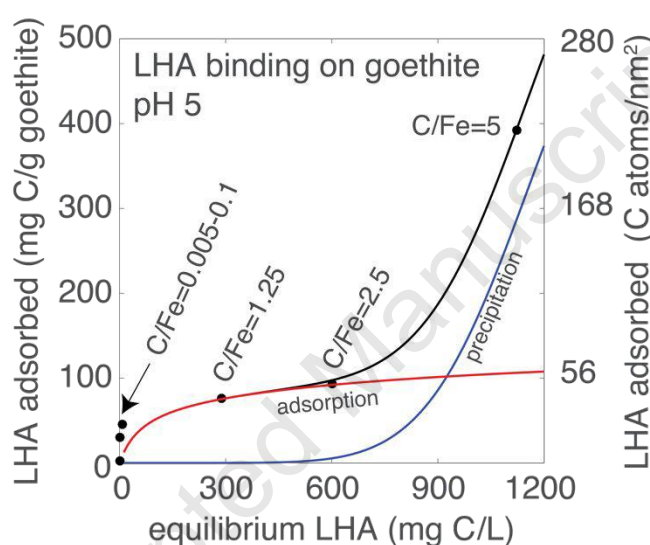
193   **Figure 1**. LHA binding on goethite after equilibration at pH 5. Total C/Fe ratios are expressed in terms of adsorption and
194   precipitated LHA. The model was generated using Eq.2, here adapted for the case of LHA binding and precipitation on
195   goethite.

196

197   Water vapor binding on goethite follows the characteristics of Type II[33] adsorption isotherms, and is

198   strongly affected by LHA loadings (Figures 2a-b). LHA loadings in the C/Fe = 0.005 - 0.01 range decreased

199   goethite hydrophilicity, while loadings above this this range increased hydrophilicity. Water uptake of

200   unbound LHA is highest due to its heterogeneous structure and abundant hydrophilic functional groups. As a

201   result, increasing excess LHA loadings promotes water uptake.

202

203

204   These changes can be appreciated further by decomposing these adsorption isotherms in terms of (*i*)

205   *adsorption* and (*ii*) *condensation* regimes (Figure 2a), using Do & Do[30] theory (Eq. 2) presented in Section

206   2.3.3. In this framework, *adsorption* pertains to the attachment of water molecules to mineral surface and LHA

207   functional groups via hydrogen bonding, followed by growth in the neighborhood of the adsorption site, very

208   much in the manner described by B.E.T. theory.[32] *Condensation*, on the other hand, pertains to water-water

209   interactions leading to growth and coalescence of water (nano)droplets in (nano)/(micro)pores between

210   goethite particles and within the LHA bulk.[33]

211

212   Modeling of the water adsorption isotherms shows that maximal densities achieved under the adsorption

213   regime on LHA-free goethite are equivalent to the total crystallographic O surface density (~15

214   H_2O/nm^2)[27,31,32], and therefore ~1-1.5 H_2O monolayers. These loadings are however strongly affected by LHA

215   loadings, as shown by the relationship of Figure 2c. This correlation expresses the decreased hydrophilicity

216   of goethite at C/Fe below ~0.24 and of the increased hydrophilicity above these loadings. A mechanistic

217   interpretation of these results can be developed by understanding the nature of organic-mineral interactions,

218   and of hydrogen bonding of water on LHA-coated goethite. This can be gained by following the changes in

219   the availability of the hydrophilic hydroxyl functional groups on goethite, as well as those of LHA (Figure 3),

220   as will be detailed in the following paragraphs.

221
222
223
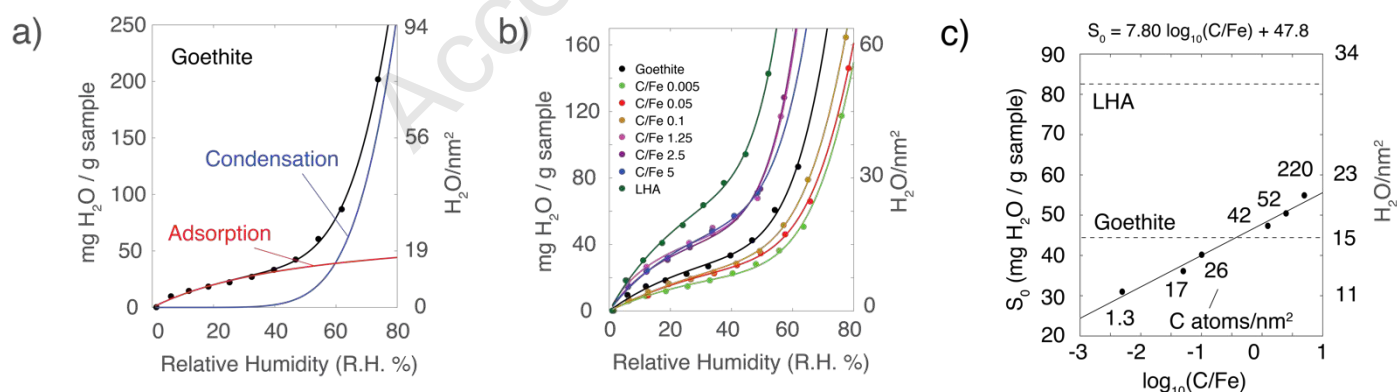
224
225 **Figure 2.** QCM-derived masses of water uptake by LHA and goethite. **(a)** Typical Type II water sorption isotherm on pure
226 goethite. **(b)** Sorption isotherms for pure goethite, LHA and goethite-LHA, reported as total C/Fe (w/w). **(c)** Relationship
227 between water site density (S_0 of Eq. 2) and total carbon loading on goethite (C/Fe). Values for pure goethite and LHA are
228 shown for reference.

229

230

231
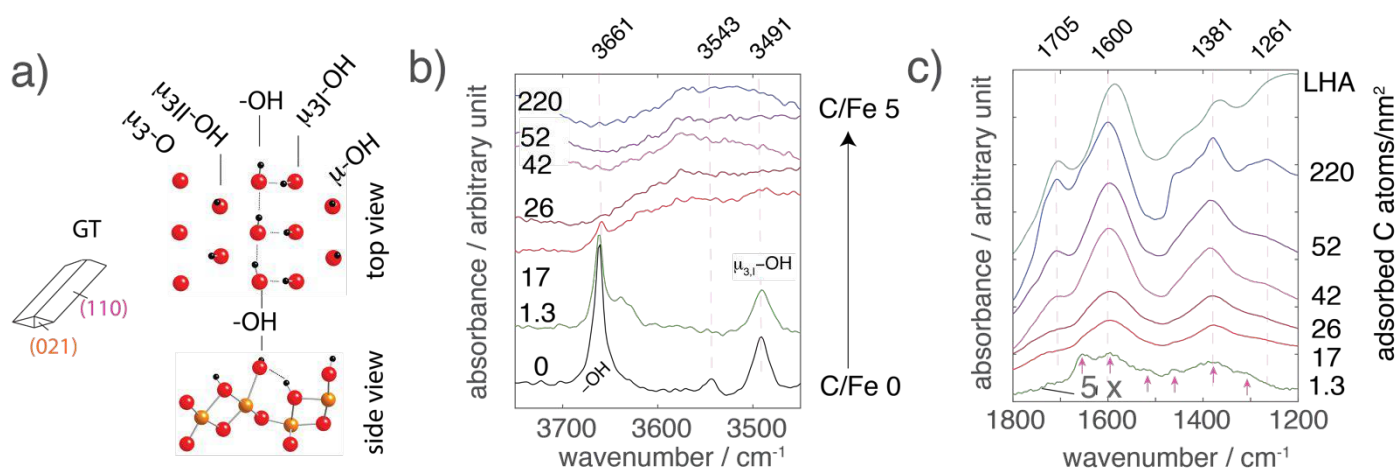
Figure 3. (a). Schematic representation of crystal habits of goethite (GT) particles under study, obtained from a selected portion of a snapshot of a Molecular Dynamics simulation from a previous study.[18] **(b-c)** FTIR spectra of LHA-Goethite samples equilibrated at pH 5 then dried under $N_2(g)$. **(c)** Difference spectra of the 1200-1800 cm^{-1} region, with removed contributions from the goethite bulk ($\delta_{OH}+\gamma_{OH}$ = 1659 cm^{-1}; δ'_{OH}=1794 cm^{-1}; *cf.* Figure S1 for raw data). Arrows in 1.3 adsorbed C atoms/nm^2 point to collection of bands.

239   Changes in the availability of hydrophilic hydroxo groups populating the goethite surface (Fig. 3a) can

240   be revealed by vibrational spectroscopy (Fig. 3b), a detailed account of which is given in a series of articles

241   from our group.[17–19,22,36,37] Briefly, the dominant (110) crystallographic face of goethite populated by rows of

242   singly-coordinated −OH, doubly-coordinated μ−OH, and triply-coordinated μ_3−OH groups. About 50% of

243   these −OH donate a hydrogen bond to a neighboring −OH, while all accept a hydrogen bond from an

244   underlying $\mu_{3,I}$−OH, as in the goethite bulk. [17–19,22,36,37] The intensities and positions of O-H stretching bands

245   of −OH groups (3661 cm^{-1}) and of the less reactive μ−OH and $\mu_{3,I}$−OH groups (3648 cm^{-1}) are especially

246   sensitive indicators of ligand exchange and hydrogen bonding reactions. Variations in the intensities of the

247   triply-coordinated $\mu_{3,I}$−OH sites (3491 cm^{-1}) are, in turn, a direct response of the coordination changes in −OH

248   due to the presence of a hydrogen bond between these two groups ($\mu_{3,I}$−OH···OH−). Finally, we note that

249   while the minor (021) face also exposes −OH and μ−OH groups they are so strongly hydrogen-bonded that

250   they generate no resolvable O-H stretch, as described in Song and Boily.[17]

251

252   The loss in intensity of these O-H stretching bands in the C/Fe 0 - 0.1 range confirms the loss of hydrophilic

253   −OH groups via ligand exchanges and/or the loss of the hydrophilic activity of these groups via hydrogen

254   bonding with LHA functional groups.[25, 37–39] These changes correlate with the appearance of LHA functional

255   groups in the range of 1200-1800 cm^{-1} (Figure 3c), which we interpret as the appearance of a mixture of

256   protonated ($\upsilon_{C=O\ carboxyl}$ = 1705 cm^{-1}, υ_{C-O-H} = 1261 cm^{-1}) and deprotonated (υ_{COOs} = 1381 cm^{-1}) groups, as

257   well as aromatic backbone of LHA ($\upsilon_{C=C}$ aromatic = 1600 cm^{-1}). They also reveal that the LHA-reacted

1

258 goethite surface exposes a mixture of −OH groups and of LHA. At C loadings greater than the crystallographic

259 density of goethite surface oxygens (> 26 C atoms/nm^2; C/Fe > 0.1), all intensities of the −OH band are lost

260 due to direct ligand exchange with LHA and a red-shift in the stretching frequency of hydrogen-bonded group

261 to a broad range of values below 3661 cm^{-1}. The O-H spectral signature is then characterized by a blue-shift

262 in the band of $\mu_{3,I}$−OH from the weakening of its hydrogen bond with −OH, as well as from the appearance

263 of OH groups of sorbed LHA. Additionally, because LHA loadings increased under conditions where all -OH

264 groups have been occupied, LHA binding must have been driven by additional mechanisms such as van der

265 Waals-type hydrophobic bonding. This mechanism could be responsible for the precipitation of LHA at the

266 highest loadings considered in this work (Fig. 1).

267
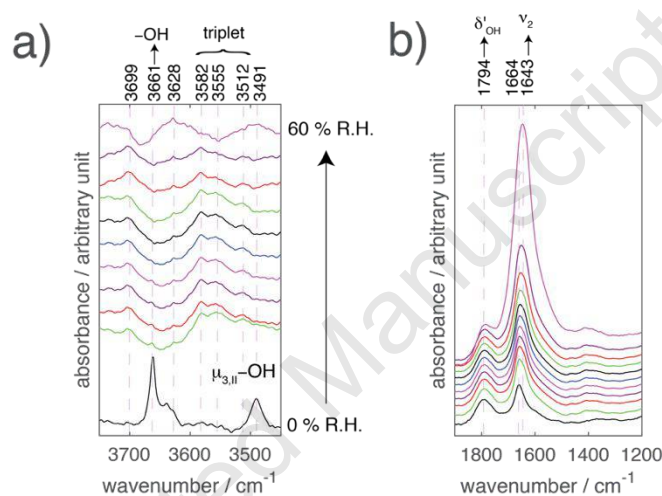
268 **Figure 4.** Baseline-subtracted FTIR spectra of C/Fe = 0.005 exposed to 0-60 % R.H. **(a)** O-H stretching region responding to
269 -OH and μ_{3I}-OH groups. The 3699 cm^{-1} band is likely from geminal water bound directly to Fe sites, but is outside the scope
270 of this work. **(b)** The 1200-1900 cm^{-1} region. This region shows the appearance of liquid-like water through the growth of the
271 bending band of water (ν_2). The δ'_{OH} 1794 cm^{-1} band is an bending overtone of the goethite bulk, and therefore not affected
272 by water binding.
273
274
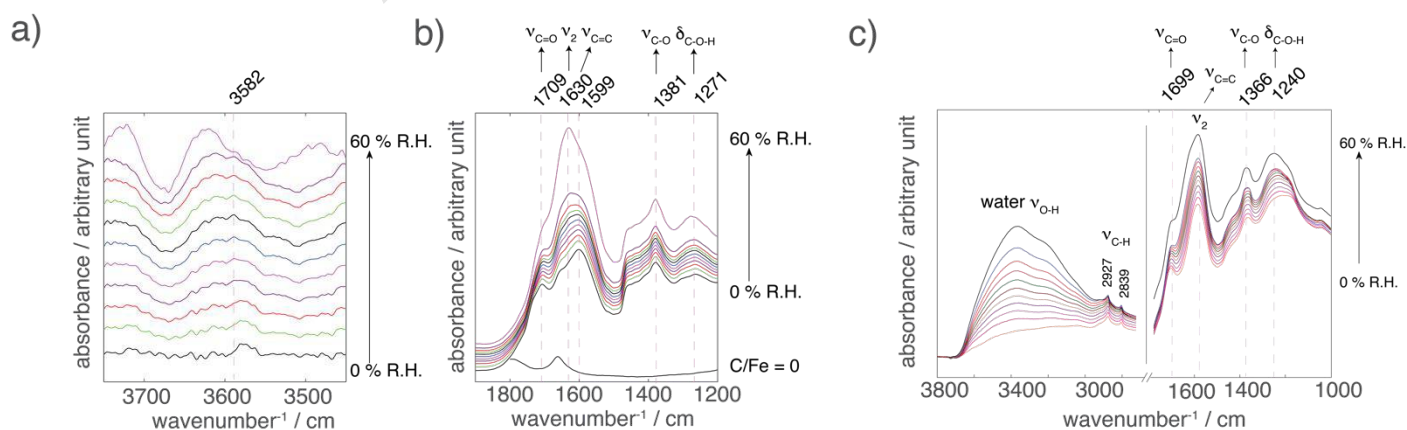
275
276
277 **Figure 5. (a-b)** Baseline-subtracted FTIR spectra of C/Fe = 5 exposed to 0-60 % R.H. **(c)** FTIR spectra of LHA first
278 equilibrated at pH 5, then exposed to water vapor.

1

279

280   Exposure of water vapor to LHA-coated goethite (Fig. 4 & 5) also induced systematic changes in the

281   vibration spectra of goethite and LHA functional groups, and generated bands strongly indicative of the

282   formation of liquid-like water. [41,42] While this can first be appreciated by the appearance of the bending (ν_2;

283   Fig. 4b) and of the broad O-H stretching (Fig. 5c) bands of water deposited within the three-dimensional

284   framework of LHA (see also Figs S3 & S4), the spectral signature of hydrophilic OH groups provide greater

285   details on water condensation mechanisms.

286

287   Samples with the lowest LHA loadings (C/Fe = 0.005) provide insight into the mechanisms of water

288   binding at goethite surfaces exposing a mixture of (*i*) non-reacted −OH groups and (*ii*) adjacently-bound LHA

289   molecules. While our results (Fig. 2) showed that water loadings were *lower* than on LHA-free goethite,

290   vibration spectra (Fig. 4) suggest that water binding mechanisms were not altered by LHA-binding.[18] This can

291   be appreciated in the loss and red-shift of the 3661 cm^{-1} band of –OH with water loading, as well as in the

292   blue-shift of the 3490 cm^{-1} band of $\mu_{3,I}$−OH to a triplet at 3512, 3555, and 3582 cm^{-1}, also seen in LHA-free

293   goethite.[18] We note that this triplet results from a weakening of the H-bonding strength between $\mu_{3,I}$−OH and

294   −OH sites by water through the formation of hydrogen bonding networks of the type: $\mu_{3,I}$−OH$\cdots$−OH$\cdots$−OH$_2$

295   and/or $\mu_{3,I}$−OH$\cdots$−OH$_2$. As water-binding mechanisms remain unchanged by LHA, lower water loadings are

296   likely to result from the consumption of hydrophilic sites by LHA surface complexation, for example via

297   ligand exchange and/or hydrogen bonding.   This could also imply that the intrinsic LHA bulk structure (*e.g.*,

298   intramolecular hydrogen bonding network) has undergone changes that, for example, expose hydrophobic

299   sites to the outer portion of the macromolecules. This concept can be supported further in the 1200-1800 cm^{-}

300   ^{1} region (Fig. 3c) revealing a combination of bands that is not manifested at larger LHA loadings. Previous

301   work from our group even showed that these conformational changes could be responsible for increasing the

302   thermal stability of mineral-bound NOM.

303

304   This scenario diverges starkly with water binding to samples of high C/Fe loadings which, again, promote

305   greater water loadings than in LHA-free goethite (Fig. 2). In this case, the aforementioned triplet (Fig. 4a) is

306   readily transformed to a broad singlet, which is characteristic of a broad distribution of hydrogen bonding

307   environments (Fig. 5a). We also note that the water vapor pressure dependence of the 1200-1800 cm^{-1} region

1

308　is also considerably less sensitive than that of pure LHA (Fig. 5). This suggests that LHA functional groups

309　directly bound to goethite remain largely unaffected by hydration. It also implies that while water condensation

310　in the three-dimensional array of pure LHA facilitates high water loadings, LHA binding to goethite limits

311　this intrinsic capability to accommodate water.

312

313　To summarize, we can explain the strong LHA-loading dependence on water binding in the following

314　manner. LHA binding at low loadings (1.3-26 C atoms/nm^2; C/Fe = 0.005 - 0.1) involves a greater proportion

315　of LHA moieties for ligand exchange or hydrogen bonding to goethite surfaces. This results in potentially

316　important configurational changes in LHA structure, perhaps even exposing hydrophobic portions of the

317　molecule to the goethite surface. This, with the decrease in accessible hydrophilic groups of the goethite

318　surface, collectively lowers water binding on goethite reacted LHA loadings below ~240 mg C per g Fe. Water

319　affinities become, in turn, substantially larger at high C/Fe loadings because a smaller fraction of the moieties

320　is dedicated to binding with goethite, leaving excess LHA reacting with water in a similar manner to pure

321　LHA.

322

323　Finally, we note that while this work on water condensation in NOM-reacted minerals was limited to a

324　model system, we anticipate that its findings should be applicable to a wider range of representative systems.

325　Recognition of the NOM loading dependency on the hygroscopic properties of solid materials in nature should

326　not only be of importance to the study of terrestrial environments but also in the study of atmospheric clouds

327　and rain formation phenomena[43,44] Additionally, the molecular-scale knowledge of water vapor binding in

328　organic-mineral assemblages should serve to consolidate our understanding of natural photocatalytic

329　reactions[45] where co-adsorbed water is an essential ingredient in photodegradation processes.[46]

ACKNOWLEDGEMENTS

REFERENCES

335 (1) Matějková, š.; Šimon, T. Application of FTIR Spectroscopy for Evaluation of
336 Hydrophobic/Hydrophilic Organic Components in Arable Soil. *Plant Soil Environ.* **2012**, *58* (No. 4),
337 192–195. https://doi.org/10.17221/317/2011-PSE.

338 (2) Nebbioso, A.; Piccolo, A. Molecular Characterization of Dissolved Organic Matter (DOM): A Critical
339 Review. *Anal. Bioanal. Chem.* **2013**, *405* (1), 109–124. https://doi.org/10.1007/s00216-012-6363-2.

340 (3) Piccolo, A. The Nature of Soil Organic Matter and Innovative Soil Managements to Fight Global
341 Changes and Maintain Agricultural Productivity. *Carbon Sequestration Agric. Soils Multidiscip.*
342 *Approach Innov. Methods* **2012**. https://doi.org/10.1007/978-3-642-23385-2_1.

343 (4) Perminova, I. V.; Frimmel, F. H.; Kudryavtsev, A. V.; Kulikova, N. A.; Abbt-Braun, G.; Hesse, S.;
344 Petrosyan, V. S. Molecular Weight Characteristics of Humic Substances from Different Environments
345 As Determined by Size Exclusion Chromatography and Their Statistical Evaluation. *Environ. Sci.*
346 *Technol.* **2003**, *37* (11), 2477–2485. https://doi.org/10.1021/es0258069.

347 (5) Vindedahl, A. M.; Stemig, M. S.; Arnold, W. A.; Penn, R. L. Character of Humic Substances as a
348 Predictor for Goethite Nanoparticle Reactivity and Aggregation. *Environ. Sci. Technol.* **2016**, *50* (3),
349 1200–1208. https://doi.org/10.1021/acs.est.5b04136.

350 (6) Kaiser, K.; Guggenberger, G. Mineral Surfaces and Soil Organic Matter. *Eur. J. Soil Sci. 54* (2), 219–
351 236. https://doi.org/10.1046/j.1365-2389.2003.00544.x.

352 (7) Chassé, A. W.; Ohno, T.; Higgins, S. R.; Amirbahman, A.; Yildirim, N.; Parr, T. B. Chemical Force
353 Spectroscopy Evidence Supporting the Layer-by-Layer Model of Organic Matter Binding to Iron
354 (Oxy)Hydroxide Mineral Surfaces. *Environ. Sci. Technol.* **2015**, *49* (16), 9733–9741.
355 https://doi.org/10.1021/acs.est.5b01877.

356 (8) Philippe, A.; Schaumann, G. E. Interactions of Dissolved Organic Matter with Natural and Engineered
357 Inorganic Colloids: A Review. *Environ. Sci. Technol.* **2014**, *48* (16), 8946–8962.
358 https://doi.org/10.1021/es502342r.

359 (9) Chi, F.-H.; Amy, G. L. Kinetic Study on the Sorption of Dissolved Natural Organic Matter onto
360 Different Aquifer Materials: The Effects of Hydrophobicity and Functional Groups. *J. Colloid Interface*
361 *Sci.* **2004**, *274* (2), 380–391. https://doi.org/10.1016/j.jcis.2003.12.049.

362 (10) Smith, K. E. C.; Thullner, M.; Wick, L. Y.; Harms, H. Dissolved Organic Carbon Enhances the Mass
363 Transfer of Hydrophobic Organic Compounds from Nonaqueous Phase Liquids (NAPLs) into the
364 Aqueous Phase. *Environ. Sci. Technol.* **2011**, *45* (20), 8741–8747. https://doi.org/10.1021/es202983k.

365 (11) Situm, A.; Rahman, M. A.; Allen, N.; Kabengi, N.; Al-Abadleh, H. A. ATR-FTIR and Flow
366 Microcalorimetry Studies on the Initial Binding Kinetics of Arsenicals at the Organic–Hematite
367 Interface. *J. Phys. Chem. A* **2017**, *121* (30), 5569–5579. https://doi.org/10.1021/acs.jpca.7b03426.

(12)   Strathmann, T. J.; Stone, A. T. Reduction of Oxamyl and Related Pesticides by FeII: Influence of Organic Ligands and Natural Organic Matter. *Environ. Sci. Technol.* **2002**, *36* (23), 5172–5183. https://doi.org/10.1021/es0205939.

(13)   Iglesias, A.; López, R.; Gondar, D.; Antelo, J.; Fiol, S.; Arce, F. Adsorption of Paraquat on Goethite and Humic Acid-Coated Goethite. *J. Hazard. Mater.* **2010**, *183* (1), 664–668. https://doi.org/10.1016/j.jhazmat.2010.07.077.

(14)   Weng, L.; Van Riemsdijk, W. H.; Hiemstra, T. Cu2+ and Ca2+adsorption to Goethite in the Presence of Fulvic Acids. *Geochim. Cosmochim. Acta* **2008**, *72* (24), 5857–5870. https://doi.org/10.1016/j.gca.2008.09.015.

(15)   Murphy, E. M.; Zachara, J. M.; Smith, S. C. Influence of Mineral-Bound Humic Substances on the Sorption of Hydrophobic Organic Compounds. *Environ. Sci. Technol.* **1990**, *24* (10), 1507–1516. https://doi.org/10.1021/es00080a009.

(16)   Capriel, P.; Beck, T.; Borchert, H.; Gronholz, J.; Zachmann, G. Hydrophobicity of the Organic Matter in Arable Soils. *Soil Biol. Biochem.* **1995**, *27* (11), 1453–1458. https://doi.org/10.1016/0038-0717(95)00068-P.

(17)   Song, X.; Boily, J.-F. Structural Controls on OH Site Availability and Reactivity at Iron Oxyhydroxide Particle Surfaces. *Phys. Chem. Chem. Phys.* **2012**, *14* (8), 2579–2586. https://doi.org/10.1039/C2CP22715K.

(18)   Song, X.; Boily, J.-F. Water Vapor Adsorption on Goethite. *Environ. Sci. Technol.* **2013**, *47* (13), 7171–7177. https://doi.org/10.1021/es400147a.

(19)   Song, X.; Boily, J.-F. Water Vapor Interactions with FeOOH Particle Surfaces. *Chem. Phys. Lett.* **2013**, *560*, 1–9. https://doi.org/10.1016/j.cplett.2012.12.048.

(20)   Feng, W.; Klaminder, J.; Boily, J.-F. Thermal Stability of Goethite-Bound Natural Organic Matter Is Impacted by Carbon Loading. *J. Phys. Chem. A* **2015**, *119* (51), 12790–12796. https://doi.org/10.1021/acs.jpca.5b09821.

(21)   Boily, J.-F. Water Structure and Hydrogen Bonding at Goethite/Water Interfaces: Implications for Proton Affinities. *J. Phys. Chem. C* **2012**, *116* (7), 4714–4724. https://doi.org/10.1021/jp2110456.

(22)   Boily, J.-F.; Szanyi, J.; Felmy, A. R. A Combined FTIR and TPD Study on the Bulk and Surface Dehydroxylation and Decarbonation of Synthetic Goethite. *Geochim. Cosmochim. Acta* **2006**, *70* (14), 3613–3624. https://doi.org/10.1016/j.gca.2006.05.013.

(23)   Hur, J.; Schlautman, M. A. Molecular Weight Fractionation of Humic Substances by Adsorption onto Minerals. *J. Colloid Interface Sci.* **2003**, *264* (2), 313–321. https://doi.org/10.1016/S0021-9797(03)00444-2.

(24)   Qin, X.; Liu, F.; Wang, G.; Hou, H.; Li, F.; Weng, L. Fractionation of Humic Acid upon Adsorption to Goethite: Batch and Column Studies. *Chem. Eng. J.* **2015**, *269*, 272–278. https://doi.org/10.1016/j.cej.2015.01.124.

(25)   Kang, S.; Xing, B. Humic Acid Fractionation upon Sequential Adsorption onto Goethite. *Langmuir* **2008**, *24* (6), 2525–2531. https://doi.org/10.1021/la702914q.

(26)   M. Vindedahl, A.; H. Strehlau, J.; A. Arnold, W.; Lee Penn, R. Organic Matter and Iron Oxide Nanoparticles: Aggregation, Interactions, and Reactivity. *Environ. Sci. Nano* **2016**, *3* (3), 494–505. https://doi.org/10.1039/C5EN00215J.

(27)   Gaboriaud, F.; Ehrhardt, J.-J. Effects of Different Crystal Faces on the Surface Charge of Colloidal Goethite (α-FeOOH) Particles: An Experimental and Modeling Study. *Geochim. Cosmochim. Acta* **2003**, *67* (5), 967–983.
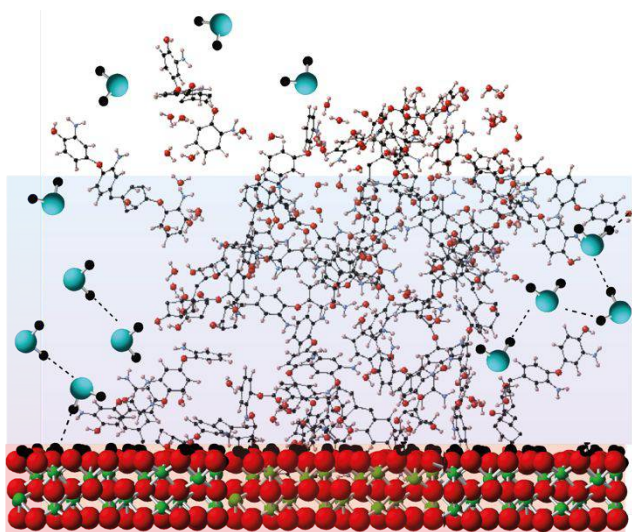
(28) Marsac, R.; Martin, S.; Boily, J.-F.; Hanna, K. Oxolinic Acid Binding at Goethite and Akaganéite Surfaces: Experimental Study and Modeling. *Environ. Sci. Technol.* **2016**, *50* (2), 660–668. https://doi.org/10.1021/acs.est.5b04940.

(29) Sauerbrey, G. Verwendung von Schwingquarzen zur Wägung dünner Schichten und zur Mikrowägung. *Z. Für Phys.* **1959**, *155* (2), 206–222. https://doi.org/10.1007/BF01337937.

(30) Do, D. D.; Do, H. D. A Model for Water Adsorption in Activated Carbon. *Carbon* **2000**, *38* (5), 767–773. https://doi.org/10.1016/S0008-6223(99)00159-1.

(31) Yeşilbaş, M.; Boily, J.-F. Particle Size Controls on Water Adsorption and Condensation Regimes at Mineral Surfaces. *Sci. Rep.* **2016**, *6*, 32136. https://doi.org/10.1038/srep32136.

(32) Brunauer, S.; Emmett, P. H.; Teller, E. Adsorption of Gases in Multimolecular Layers. *J. Am. Chem. Soc.* **1938**, *60* (2), 309–319. https://doi.org/10.1021/ja01269a023.

(33) Sing, K. S. W. Reporting Physisorption Data for Gas/Solid Systems with Special Reference to the Determination of Surface Area and Porosity (Recommendations 1984). *Pure Appl. Chem.* **1985**, *57* (4), 603–619. https://doi.org/10.1351/pac198557040603.

(34) Hiemstra, T.; Van Riemsdijk, W. H. A Surface Structural Approach to Ion Adsorption: The Charge Distribution (CD) Model. *J. Colloid Interface Sci.* **1996**, *179* (2), 488–508.

(35) Boily, J.-F.; Felmy, A. R. On the Protonation of Oxo- and Hydroxo-Groups of the Goethite (α-FeOOH) Surface: A FTIR Spectroscopic Investigation of Surface O–H Stretching Vibrations. *Geochim. Cosmochim. Acta* **2008**, *72* (14), 3338–3357. https://doi.org/10.1016/j.gca.2008.04.022.

(36) Ding, X.; Song, X.; Boily, J.-F. Identification of Fluoride and Phosphate Binding Sites at FeOOH Surfaces. *J. Phys. Chem. C* **2012**, *116* (41), 21939–21947. https://doi.org/10.1021/jp3083776.

(37) Kanematsu, M.; Waychunas, G. A.; Boily, J.-F. Silicate Binding and Precipitation on Iron Oxyhydroxides. *Environ. Sci. Technol.* **2018**, *52* (4), 1827–1833. https://doi.org/10.1021/acs.est.7b04098.

(38) Gu, B.; Schmitt, J.; Chen, Z.; Liang, L.; McCarthy, J. F. Adsorption and Desorption of Different Organic Matter Fractions on Iron Oxide. *Geochim. Cosmochim. Acta* **1995**, *59* (2), 219–229. https://doi.org/10.1016/0016-7037(94)00282-Q.

(39) Fu, H.; Quan, X. Complexes of Fulvic Acid on the Surface of Hematite, Goethite, and Akaganeite: FTIR Observation. *Chemosphere* **2006**, *63* (3), 403–410. https://doi.org/10.1016/j.chemosphere.2005.08.054.

(40) Gu, B.; Schmitt, J.; Chen, Z.; Liang, L.; McCarthy, J. F. Adsorption and Desorption of Natural Organic Matter on Iron Oxide: Mechanisms and Models. *Environ. Sci. Technol.* **1994**, *28* (1), 38–46. https://doi.org/10.1021/es00050a007.

(41) Ghabbour, E. A.; Davies, G. *Humic Substances: Structures, Models and Functions*; Royal Society of Chemistry, 2007.

(42) Senesi, N.; Miano, T. M.; Provenzano, M. R.; Brunetti, G. Spectroscopic and Compositional Comparative Characterization of I.H.S.S. Reference and Standard Fulvic and Humic Acids of Various Origin. *Sci. Total Environ.* **1989**, *81–82*, 143–156. https://doi.org/10.1016/0048-9697(89)90120-4.

(43) Levin, Z.; Teller, A.; Ganor, E.; Yin, Y. On the Interactions of Mineral Dust, Sea-Salt Particles, and Clouds: A Measurement and Modeling Study from the Mediterranean Israeli Dust Experiment Campaign. *J. Geophys. Res. Atmospheres* **2005**, *110* (D20202), 1–19. https://doi.org/10.1029/2005JD005810.

(44) Noziere, B. Don't Forget the Surface. *Science* **2016**, *351* (6280), 1396–1397. https://doi.org/10.1126/science.aaf3253.

456 (45) Cwiertny, D. M.; Young, M. A.; Grassian, V. H. Chemistry and Photochemistry of Mineral Dust
457 Aerosol. *Annu. Rev. Phys. Chem.* **2008**, *59* (1), 27–51.
458 https://doi.org/10.1146/annurev.physchem.59.032607.093630.
459 (46) Mino, L.; Zecchina, A.; Martra, G.; Rossi, A. M.; Spoto, G. A Surface Science Approach to TiO2 P25
460 Photocatalysis: An in Situ FTIR Study of Phenol Photodegradation at Controlled Water Coverages from
461 Sub-Monolayer to Multilayer. *Appl. Catal. B Environ.* **2016**, *196*, 135–141.
462 https://doi.org/10.1016/j.apcatb.2016.05.029.

463
464
465
466
467
468
469
470
471
472
473
474
475
476
477
478
479
480
481
482
483
484
485
486
487
488
489
490
491
492
493
494

495 **Graphical Abstract**

496

497